

Raman spectroscopic characterization of a Martian SNC meteorite: Zagami

Alian Wang, Bradley L. Jolliff, and Larry A. Haskin

Department of Earth and Planetary Sciences and McDonnell Center for the Space Sciences, Washington University, St. Louis, Missouri

Abstract. To demonstrate the ability of Raman spectroscopy to determine the mineralogical character of a rock that originated on Mars, we analyzed a small slab of “normal Zagami” by point analyses and multipoint scans using laboratory spectrometers. Spectra of clinopyroxenes were dominant; their compositions were estimated from a calibration of Raman peak positions with Mg/(Mg+Fe) based on lunar pyroxenes of known composition, and these agree with compositions obtained by electron microprobe. A few spectra of orthopyroxene were observed. The broad spectrum of maskelynite was observed, but not that of plagioclase feldspar. Spectra of minor phosphates, magnetite, and pyrrhotite were obtained, as were spectra of an organic contaminant and of hematite, both apparently introduced during sample handling prior to Raman analysis. The modal analysis based on the multipoint scans agrees well with published values. If the spectra had been obtained on the surface of Mars by Raman spectroscopic analysis as a stand-alone method and no other information about the sample was available (and by ignoring the spurious hematite and organic material), we could rule out sedimentary and plutonic rock types and conclude that the sample was a pyroxene-phyric basalt.

1. Introduction

We advocate rover-based Raman spectrometers as a means to obtain detailed, in situ mineral characterization of materials on planetary surfaces [Wang *et al.*, 1995, 1998]. Given that a series of landed missions to Mars is planned, with the intent to collect samples for transport to Earth, we are investigating what a rover-based Raman spectrometer could tell us about materials found on the Martian surface. We have previously shown that a miniaturized Raman system could identify major and minor minerals in rocks, determine mineral proportions in rocks and soils, enable identification of rock types, determine cation ratios in certain minerals, provide first-order information about rock texture (the spatial distribution of mineral phases, the presence of veins, etc.), and identify alteration products of primary minerals [Haskin *et al.*, 1997].

In this study, we demonstrate that in an actual Martian rock, the Zagami meteorite, major minerals (pyroxene and maskelynite) and minor and trace minerals (merrillite (whitlockite), apatite, pyrrhotite, and magnetite) can be identified by using a Raman system and a measurement procedure similar to those we anticipate using for in situ Raman analysis on the surface of Mars. By Raman point-counting, we have obtained a mineral mode of the Zagami sample that is consistent with literature values. We have also obtained a distribution of Mg/Fe ratios in Zagami pyroxenes reflecting the chemical zoning of individual grains. We were able to deduce from the information obtained that the Zagami rock sample has a texture consistent with a coarse, pyroxene-rich basalt containing interstitial maskelynite and mesostasis. This study supports our contention that in situ Raman measurements on Mars surface samples can provide good first-order characterization of these lithologic components.

2. Sample and Experiments

2.1. The Sample

Zagami, one of the basaltic Shergottites, fell in 1962 in Nigeria and was subsequently cut up and distributed widely (summarized by Meyer [1996]). Weighing 18 kg, the Zagami meteorite is a heterogeneous rock that contains several texturally distinct lithologies. Overall, it is fine to medium grained and has basaltic composition and mineralogy. Most of the meteorite consists of so-called “normal Zagami” (NZ) lithology, which is pyroxene-rich and has a diabasic or subophitic texture similar to that of Shergotty [Stolper and McSween, 1979; McCoy *et al.*, 1992]. Judging from one of the large remaining specimens, roughly 20% of the meteorite consists of a dark, mottled lithology (DML), which is separated from NZ by a sharp but irregular contact [McCoy *et al.*, 1995]. The DML contains a fayalite-bearing lithology referred to as Zagami DN (originally found in a sample from David New, reported by Vistisen *et al.*, [1992]; see McCoy *et al.*, [1995]), which appears to represent a related, late-stage melt pocket. The DML also contains pockets of shock melt that have yielded traces of Martian atmosphere [Marti *et al.*, 1995]. McCoy *et al.* [1992, 1995] also report the occurrence of veins of shock melt and of maskelynite that transect NZ. On the basis of mineral compositions and assemblages, the three lithologies, NZ – DML – DN, appear to be related to one another by a fractionation sequence [McCoy *et al.*, 1995]. The specimen that we analyzed consisted entirely of the NZ lithology.

The Zagami NZ lithology typically exhibits a foliated texture, consisting of a pronounced alignment of pyroxene grains and maskelynite [Stolper and McSween, 1979; McCoy *et al.*, 1992], with maskelynite generally occupying interstices between pyroxene grains. The composition of Zagami is approximately that of a low-alumina basalt. Stolper and McSween [1979], however, showed that Zagami has an accumulation of pyroxene relative to an equilibrium, low-pressure magmatic liquid containing pigeonite and plagioclase of appropriate composition. They inter-

Copyright 1999 by the American Geophysical Union

Paper number 1999JE900004.
0148-0227/99/1999JE900004\$09.00

Zagami

scale: ~ 1.5 cm across

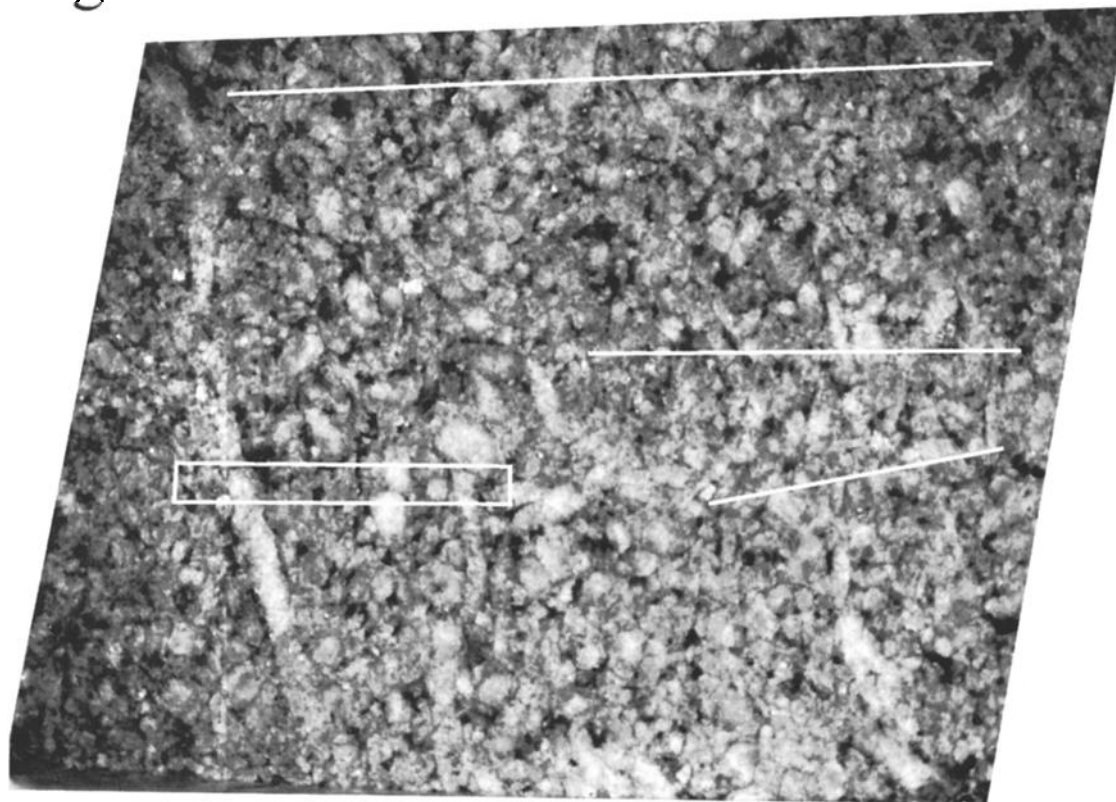


Figure 1. Photograph of sawn, lightly polished surface of Zagami, ~ 1.5 cm across (2.5 g chip lent to us for this study by Tom Wdowiak). Light-green, fractured pyroxene dominates the assemblage, with some grains reaching 3–4 mm in length and 0.3–0.4 mm across. This specimen shows clear evidence of preferential alignment of pyroxene grains and appears to be representative of the “coarse, normal Zagami” lithology. Raman point-count traverses were made along the three lines as shown, and a grid of spot analyses was done in the area outlined by the rectangle.

preted this accumulation as a result of gravity settling. The grain size is variable in different subsamples or areas, with averages ranging from approximately 0.2 mm (“fine-grained” portions) to 0.4 mm (“coarse-grained” portions) [McCoy *et al.*, 1992]. Within a given area, mineral proportions are variable, as follows: pyroxene (augite, pigeonite): 70–80 vol%; maskelynite, 10–20 vol%; oxides (titanomagnetite, ilmenite), 1.5–2.8 vol%; sulfide (pyrrhotite), 0.2–0.6 vol%; phosphate [Na-whitlockite (merrillite)], 0.5–1.3 vol%; mesostasis, 1.7–3.7 vol%, and shock melt, 0.1–0.9 vol% [Stolper and McSween, 1979; McCoy *et al.*, 1992;] (summarized in Table 2). Mesostasis consists of vermicular intergrowths of glass and silica with magnetite, ilmenite, fayalite, and pyrrhotite [Stolper and McSween, 1979]. Minerals that constitute the mesostasis are concentrated and coarser in the DN lithology than in NZ. In addition to merrillite, fluorapatite has been reported in DN, but not NZ [Watson *et al.*, 1994]. Magmatic melt inclusions containing amphibole have been reported in the cores of pigeonite grains [Treiman, 1985; McCoy *et al.*, 1992]; these are OH-bearing (~2 wt%), with very little F or Cl.

The sample that we analyzed is a 2.5 g, flat, rectangular sawn chip measuring roughly 1.5 × 1.0 × 0.5 cm, as shown in the bright-field photo, Figure 1. Visual examination of the Zagami specimen clearly shows a preferred orientation of elongate pyroxene grains. A few pyroxene grains are 3–4 mm in length and 0.3–0.4 mm across, and most grains are in the 0.2–0.5 mm diameter range, indicating that this specimen represents a relatively coarse

portion of NZ. Pyroxene grains are typically light green and fractured; we could not distinguish pigeonite from augite macroscopically. Initial Raman measurements were made directly on the rough sawn surface of the rock slab. For later measurements, we polished one surface lightly. The polishing had no noticeable effect on the quality of the Raman spectra, but enabled better petrographic examination of the specimen.

2.2. The Raman Spectrometers.

Two different Raman spectrometers with lasers operating at different frequencies were used for this study. Both gave comparable results. The initial measurements were done using a micro-Raman spectrometer model S3000 (Jobin-Yvon / Instrument S. A.). It has a spectrograph of Czerny-Turner configuration, coupled with a subtractive double-monochromator. It uses a diode array as multichannel detector and the 514.5nm line of an Ar⁺ laser for excitation. The rock sample to be studied is placed on the microscope stage of this instrument. A microscope objective condenses and directs the excitation laser beam onto the sampling spot. The same objective then collects the Raman scattered radiation from the sample and sends it back to the spectrometer for analysis. In this study, an 80x ultra long working distance objective (0.85 NA) was used. It produces a condensed laser beam <1 μm in diameter, although actual analyzed volumes in the rock sample were larger and varied from the spot to spot. The sam-

pling volume depends on the absorption and scattering of the laser light and Raman radiation from crystal faces and other discontinuities within the rock sample and thus is a function of the mineral species, their indices of refraction and absorption coefficients, and their grain sizes and rock textures. Depending on the phases analyzed, the laser power at the sampling spot was adjusted from ~7 mW for most mineral species to less than 2 mW for iron oxides and iron sulfide to preclude any damage from overheating. Two types of measurements were made using this instrument: examination of selected individual points, and a 40-point linear traverse at points 100 μm apart. For this traverse, the microscopic stage was moved manually. Both types of measurement were done using a tightly condensed excitation laser beam and a fine focusing adjustment at each measurement point.

Most Raman spectra of this study were taken using a HoloLab-5000-633 spectrometer system (Kaiser Optical System Inc.). The system consists of a Raman probe coupled with a microscope for sampling and a spectrograph box and a laser source. A single-mode optical fiber is used to transfer the excitation laser beam to the probe, and a multimode fiber (100 μm core diameter) sends the collected Raman radiation back into the spectrograph. The spectrograph has an axially transmissive configuration using a HoloPlex™ volume holographic grating and a volume holographic notch filter. It can provide simultaneously a wide spectral range (-177 to 4017 cm^{-1}), high spectral resolution (~4 cm^{-1}), and high light throughput. A two-dimensional (1024 \times 256 pixel) charge-coupled device (CCD) is used as the multichannel detector, and the 632.8 nm line of a He-Ne laser is used for excitation. The laser power of the HoloLab-5000 system at the sampling spot was ~9 mW, stronger than was used in the measurements using the S3000 system. No obvious overheating was observed for heat-sensitive phases. Both the lower power density of the H-5000 system at the sampling spot (and consequently, larger sampling volume) and the lower excitation frequency (632.8 nm) make overheating of the sample unlikely.

The purpose of these experiments was to simulate roughly the automated point-counting traverse, anticipated for in situ Raman measurements on unprepared surfaces on the Martian surface. The HoloLab-5000 is well suited to this type of experiment because it is equipped with an automated scanning stage, which moves in the X and Y directions perpendicular to the incident laser beam. This was used to reposition the sample automatically for scans made either along a linear traverse at selected intervals or on a rectangular grid. Furthermore, we wished to do the experiment using a Martian rock. Thus we took advantage of an opportunity to borrow the Zagami sample. A more realistic simulation would use a rock surface weathered on Mars, but no such specimens are available. A chipped surface might be a more realistic surface than a sawn one, but the available sample was a thin slab, and chipping was not an option. Some 260 Raman measurements were made using this instrument in two linear traverses and two rectangular areas. For 212 measurements on two rectangular grids, the distance between measurement points was set to be either 100 μm or 200 μm . A 20 \times long-working distance objective (0.4 NA) was used, which produces a condensed laser beam ~2 μm in diameter at the focusing plane.

We anticipate that detailed focusing adjustment is unrealistic for a flight Raman spectrometer that will be deployed by a robotic arm, so the instrument must have sufficient depth of sampling field to overcome the effects of the sampling at points positioned as much as a few millimeters out of the plane of focus of the laser beam. Thus, for the automated traverse measurements, the focusing plane of the HoloLab instrument was adjusted only at the

first point of each measurement set (traverse or grid). As no further focusing adjustment was made for subsequent measurement points, the sample surface was a little above or below the laser focusing plane at most points because of the surface roughness of the rock sample. When that occurs, the analyzed volume in the sample is made larger still because of the divergence of the defocused laser beam at sampling points. Fortunately, by using an objective with a long working distance (1 cm) and a low numerical aperture (0.4 NA) along with a relatively large-core collecting fiber (100 μm), we achieve a great enough depth of sampling field that spectra can be obtained even when focus is not optimal [Wang *et al.*, 1998]. Because of the less than perfect focusing, however, the signal to noise ratio of many of the spectra was lower than would have been the case for in-focus measurements. The results of this work show that the spectra were nevertheless acceptable. In addition, no obvious differences in quality were observed between the spectra taken from the rough-sawn surfaces and those from the lightly polished surface.

3. Mineralogical and Petrologic Information Obtained From Raman Measurements

3.1. Pyroxene

Pyroxene is the most abundant mineral in the NZ lithology of Zagami. Figure 2 shows Raman spectra of pyroxene typical of those obtained from the Zagami sample. The Raman spectral pattern of pyroxene has mainly three groups of spectral peaks, located at the following Raman shifts: (1) near 1000 cm^{-1} , (2) near 670 cm^{-1} , and (3) in the range 200 to 400 cm^{-1} . According to previous Raman spectroscopic studies on pyroxene group minerals [Dele-Dubois *et al.*, 1980, Sharma *et al.*, 1983, Sekita *et al.*, 1988], the strongest Raman pyroxene peak, near 1000 cm^{-1} , is produced by the symmetric stretching vibration of Si-O_{nb} (O_{nb} is nonbridging oxygen) within SiO₄ tetrahedra. The peaks near 670 cm^{-1} are produced by the symmetric vibrations of T-O_b-T (T = SiO₄ tetrahedron) bonding that links the tetrahedra in the pyroxene chain. The group of peaks at about 200-400 cm^{-1} were indicated by molecular dynamical model calculations [Ghose *et al.*, 1994] to be involved with lattice modes (coherent translations of ions within the crystal), and mixing of lattice modes with Si-O vibrations within the silicate anions.

There is general similarity among all pyroxene spectral patterns, but the detailed peak patterns in each spectral region and the frequency ranges of each peak are resolvably different for pyroxenes of different structural types, i.e., orthorhombic pyroxene, monoclinic pyroxene, and triclinic pyroxenoid [Wang *et al.*, 1995]. Simple inspection of a raw pyroxene spectrum is thus usually sufficient for identifying structural type. Of the 243 pyroxene spectra obtained in this study of the Zagami meteorite, nearly all have the spectral pattern of monoclinic pyroxene (Figure 2a). Only a few have the spectral pattern of orthorhombic pyroxene. The doublet in spectral region 2 with the higher-frequency Raman peak occurring above 670 cm^{-1} , plus a characteristic small peak just above 230 cm^{-1} , is indicative of orthorhombic pyroxene (Figure 2b).

In addition to the effects of structure, the frequencies of the major Raman peaks are affected by the cations that coordinate with the silicate oxy-anions, owing to their different masses, radii, and electronegativities. Raman peak shifts vary systematically with the relative proportions of Mg, Fe, and Ca, expressed as the magnesium number [$\text{Mg}' = \text{moles Mg}/(\text{moles Mg} + \text{moles Fe})$] and Wo (wollastonite, CaSiO₃) content of the

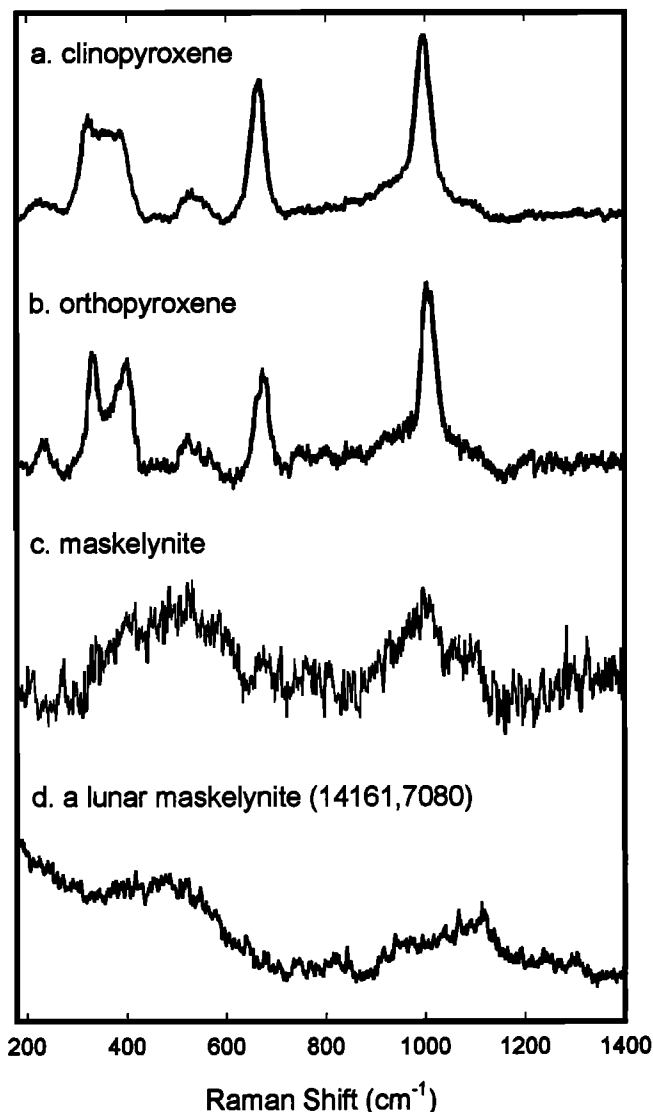


Figure 2. Typical Raman spectra of Zagami major phases: (a) clinopyroxene, (b) orthopyroxene, (c) maskelynite, and (d) lunar maskelynite.

pyroxenes, as shown in a combined Raman and electron microprobe study of lunar pyroxenes [Wang *et al.*, 1997]. We now show that the correlation found for the lunar pyroxenes also makes sense for Zagami pyroxenes.

In Figure 3a, for each Zagami pyroxene spectrum, the position of the first peak (~ 670 cm^{-1}) in spectral region 2 is plotted against the position of the third peak (~ 325 cm^{-1}) in spectral region 3 (solid symbols). Figure 3a shows many fewer points than the 243 observed. This is because the spectral peak values for many measured Zagami pyroxene grains are identical. The data for the lunar pyroxenes (open symbols) are shown in the same figure and are used to calibrate the cation ratios of the Zagami pyroxenes, whose points lie along the same broad curve observed for lunar pyroxenes. The broader spread for the Zagami pyroxenes results from somewhat less accurate peak position determination than in the lunar case because of a lower signal-to-noise ratio (S/N) in the Zagami spectra. The lunar pyroxene measurements were done on a thin section, and a high magnification objective (80x, 0.85 NA) was used with a fine focusing adjustment, producing a small

sampling volume and shallow sampling depth. Most spectra obtained were single-phase spectra with fairly high signal to noise ratio. In addition, a spectral curve fitting procedure was used to obtain the peak positions. The sampling volume and depth of sampling field are much larger for the Zagami pyroxene measurements because of the measurement conditions (described above). More multi-phase spectra were obtained, and the S/N of the Zagami pyroxene spectra was poorer and variable, which resulted in a range of accuracy (but seldom exceeding ± 1 cm^{-1}) over which the peak positions could be determined. The mild polishing of one sample surface was done to accommodate better petrographic examination, and it did not produce the quality of flatness of a thin section and did not improve the quality of the Raman spectra. The poorer focusing of the automated measurements could have contributed to the broader spread of the Zagami pyroxene data in Figure 3.

The results for all 243 pyroxene spectra are shown in the histograms of Figures 3b and 3c. These histograms illustrate the significant variation in Mg' of the Zagami pyroxenes, a consequence of compositional zoning. The position of the third peak (~ 325 cm^{-1}) changes linearly with Mg' in the range of interest, so the histogram for that peak (Figure 3b) is essentially a frequency diagram for Mg' proportional to the volume of pyroxene with each composition. At its present state of development, the measurement of pyroxene Mg' is precise to ~ 0.03 in the range of the Zagami points in Figure 3. The Mg' values lie mainly in the range 0.4–0.7, based on the lunar calibration. Among the pyroxene grains with higher Mg' (>0.6), several occur near the points for lunar orthopyroxene and, indeed, show the spectral pattern of orthorhombic pyroxene (Figure 2b). These results are consistent with the known compositions of Zagami pyroxenes. Stolper and McSween [1979] reported that Zagami pyroxenes are zoned, with Mg -rich cores and Fe -rich rims. Brearley [1991] gave the width of Fe -rich rims as typically 10–100 μm , substantial relative to the average grain size, which ranges from ~ 0.2 mm to 0.4 mm in most Zagami samples [McCoy *et al.*, 1992]. Stolper and McSween [1979] reported core compositions to be homogeneous with the following compositions: pigeonite, $\text{En}_{57.60}\text{Fs}_{31.29}\text{Wo}_{12}$ ($\text{Mg}' = 0.65$ – 0.67); augite, $\text{En}_{48}\text{Fs}_{20}\text{Wo}_{32}$ ($\text{Mg}' = 0.70$). They interpreted the core pyroxenes to be primocrysts, with Fe -rich overgrowths representing late-stage overgrowths or reaction products between accumulated primocrysts and trapped, intercumulus liquid. Some pyroxene crystals show continuous zoning from core to rim, but most apparently show a sharp transition between cores and rims [McCoy *et al.*, 1992], although intermediate compositions are well represented among published analyses [see Stolper and McSween, 1979, Figure 3]. Brearley [1991] reported pigeonite cores to be homogeneous and typically of composition $\text{En}_{60}\text{Fs}_{32}\text{Wo}_8$ ($\text{Mg}' = 0.65$ – 0.66), with rims zoned to iron-rich compositions of $\text{En}_{33}\text{Fs}_{51}\text{Wo}_{16}$ ($\text{Mg}' = 0.53$ – 0.39).

The Mg' distributions in Figure 3b thus correspond to those of the rims and cores of Zagami pyroxene grains as obtained by electron microprobe analyses [Brearley, 1991; Stolper and McSween, 1979]. A few of the pyroxene spectra are of orthorhombic pyroxene, consistent with the inversion of pigeonite as suggested by Brearley [1991]. The relatively magnesian compositions indicated by the position of the ~ 325 cm^{-1} & ~ 670 cm^{-1} peak (0.65–0.75) are consistent with these points representing core compositions; however, the most magnesian of these ($\text{Mg}' > 0.7$) is slightly more magnesian (~ 0.05 units) than any observed by others using the electron microprobe. Our calibration is self-consistent for rapidly cooled pyroxenes, and we believe it is accurate, but it appears to depend somewhat on equilibration and,

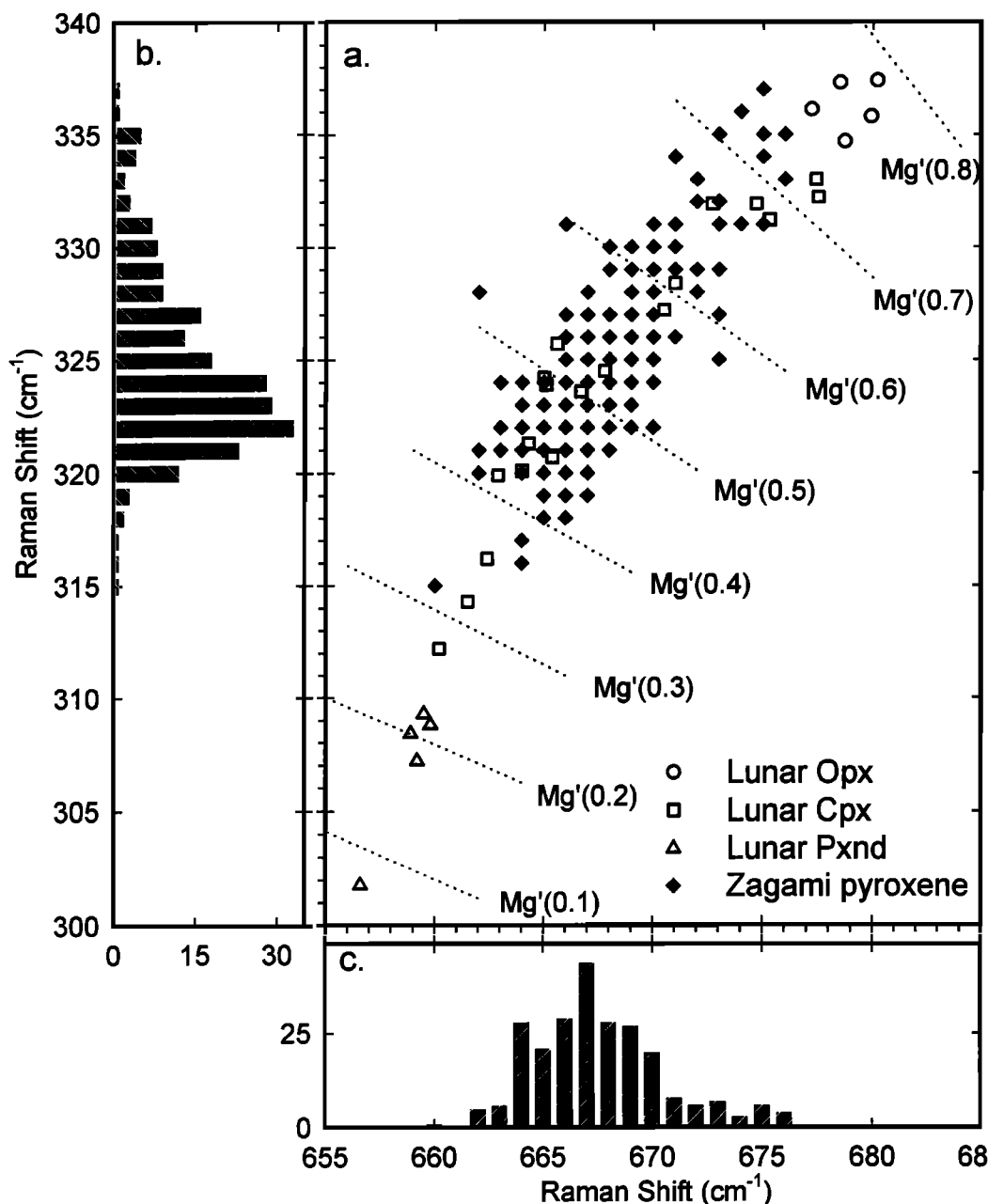


Figure 3. Compositions of Zagami pyroxene: (a) Peak positions of Zagami pyroxene are plotted on the field of lunar pyroxenes of known structural types and compositions. Values of Mg' determined for lunar pyroxene are shown. (b) Histogram of Zagami pyroxene for the third peak in spectral region 3, $\sim 325\text{ cm}^{-1}$. (c) Histogram of Zagami pyroxene for the first peak in spectral region 2, $\sim 670\text{ cm}^{-1}$.

presumably, cation ordering. The exact calibration of the Raman peak positions for Mg' , still under study, is somewhat complex and beyond the scope of this paper.

Because individual coarse pyroxene grains are readily distinguishable by visual observation in this sample of Zagami, we are able to draw conclusions about the variation in spectral peak positions (and thus Mg') as the Raman traverse crossed individual grains. Figure 4a shows the variation of Raman peak positions among the measurement points on pyroxene grains along a linear traverse of 40 points (100 μm apart) on the rough sawn surface. Peak positions for spectra from successive points on the same grain (as determined by visual observation) are connected by

dotted lines. It is obvious that the positions of the two Raman peaks ($\sim 670\text{ cm}^{-1}$ and $\sim 325\text{ cm}^{-1}$) vary sympathetically; this occurs because they both are affected by Mg' in a similar way. The peak shift tends toward lower wavenumber as Mg' decreases, so that the classic zoning pattern of Mg-rich cores grading to more Fe-rich rims should be observable. This zoning pattern is seen clearly only for the grain at the far right of the diagram (in the 3500–4000 μm range). That grain has a core with $Mg' \sim 0.7$, and in the overgrowths on both sides of the core, increasing Fe enrichment with distance from the core is seen, extending as far as $Mg' \sim 0.5$.

Such a clean-cut zoning pattern starting from a highly

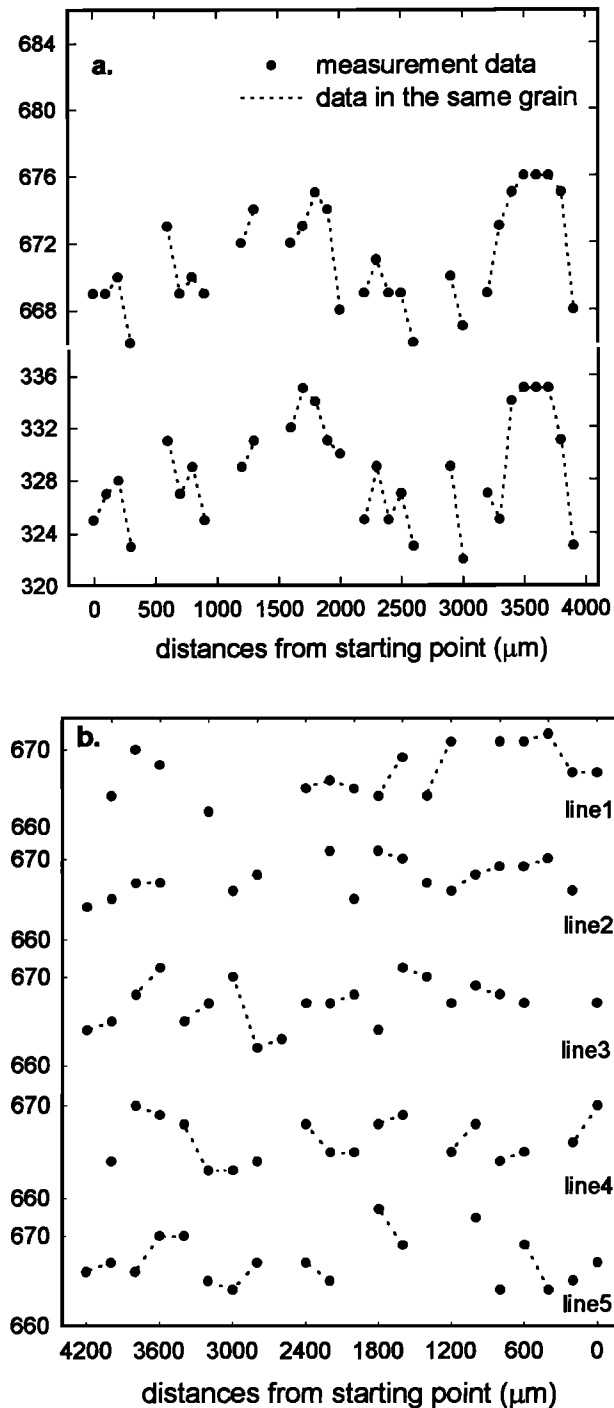


Figure 4. Spatial distribution of pyroxene Mg': (a) from spectra taken along linear traverse 1 in Figure 1 (40 points) and (b) from spectra taken in rectangular field 1 (5 rows, 22 points each) in Figure 1.

magnesian core and continuing monotonically to a more ferroan rim cannot be seen for other pyroxene grains in Figure 4a or Figure 4b. Figure 4b shows the equivalent variations in peak position of ~ 670 cm^{-1} peak from the spectra taken on a two-dimensional grid (22 points \times 5 lines). The observed irregularity is to be expected. Consider an elongate pyroxene grain, randomly oriented relative to the surface of the Zagami slab, each grain with a magnesian core and an outward-grading, more ferroan rim.

What distribution of Mg' would the Raman microbeam encounter? Only rarely would the path of the traverse cross perpendicular to a grain edge so that the classical zoning pattern of initially increasing Mg' through a core of constant Mg' to decreasing Mg' be encountered. More often, the beam would miss the core altogether (the rims are as thick or thicker than the cores) and, at interpoint distances of 100 or 200 μm , would cross, for example, a corner of a tilted grain, sampling two sides of the overgrowth unevenly and not seeing equal amounts of the two sides or obtaining the same range of Mg', still showing some systematic change in Mg' with distance. Complicated patterns of variation thus occur, with most crossings not reaching the most magnesian compositions. In addition, the laser beam penetrates into the rock matrix and scatters there in a complex way that involves indices of refraction, specular reflection, and absorption, and these affect the volume that is sampled. Effects of this type are exacerbated if the grains are not randomly oriented, as in the case of the Zagami slab. Experience in observing rocks of many textures and zoning patterns will be required to draw the maximum in accurate conclusions about a rock specimen for which no information other than a set of Raman spectra is available.

3.2. Maskelynite

All of the plagioclase in Zagami has been converted to maskelynite [Stolper and McSween, 1979], a glass of plagioclase composition formed by high shock pressure [Tschermak, 1872; Stöffler, 1974]. Compositions range from $\text{An}_{57}\text{Ab}_{42}\text{Or}_1$ to $\text{An}_{43}\text{Ab}_{53}\text{Or}_4$ with significant FeO (0.5–0.8 wt%) and MgO (0.1–0.2 wt%). The elongation and apparent alignment of maskelynite grains was interpreted by Stolper and McSween to result from crystallization of plagioclase from intercumulus melt trapped between aligned, cumulus pyroxene grains.

No Raman spectrum characteristic of plagioclase was obtained from the Zagami sample. The second most abundant type of spectra (Figure 2c) obtained were from dark, glassy grains that yielded two weak, broad Raman spectral bands. These Raman bands center at ~ 510 cm^{-1} and ~ 1000 cm^{-1} . Such features are typical of glasses consisting of framework silicates [McMillan, 1984]. We attribute this spectrum to maskelynite, the amorphous form of plagioclase produced by shock. The spectrum in Figure 2d was obtained from a lunar maskelynite grain in a thin section of 14161,7080 rock chip, and shows very similar features.

The Raman spectral features of maskelynite from different sources (a lunar meteorite, Martian meteorites, and a terrestrial impact structure) were studied by Treiman and Treado [1998] and Mikouchi *et al.* [1998]. In the study by Treiman and Treado, maskelynite from Martian meteorites ALH84001, ALHA77005,137, and EETA79001,367 all showed broad and weak spectral bands, whereas the terrestrial maskelynite from the Manicouagan impact structure had sharp Raman peaks near 500 cm^{-1} , similar to those of reference feldspar samples. In the study by Mikouchi, most maskelynite grains from the Martian meteorites Zagami, EETA79001, QUE94021, ALH77005, and Y-793605 gave broad and weak Raman bands like those we observed in Zagami maskelynite. Only the recrystallized plagioclase rims in ALH77005 yielded a Raman peak near 500 cm^{-1} , typical of plagioclase. A similar plagioclase spectral feature was observed from the maskelynite of lunar meteorite Y-793169 but not from that of A-881757, which shows only the broad bands as Martian maskelynite. In an experiment [Mikouchi *et al.* 1998], Zagami maskelynite was annealed by heating it at 900°C for 1, 4,

8, 24, and 72 hours at an f_{O_2} of iron-wustite +2. The Raman peak near 500 cm^{-1} typical of plagioclase appeared after 4 hours of annealing, and the peak intensity increased as the duration of annealing increased. The plagioclase-maskelynite relationship reflects the degree of vitrification of shocked plagioclase and the degree of subsequent annealing and thus offers information about the history of plagioclase-bearing materials subjected to shock, although it may prove complex to interpret. Also, according to Raman studies done by Heymann [1987, 1988], the increase of bandwidth of plagioclase Raman peaks and the variation of the fluorescent background can be used to evaluate shock pressure. Among the more than 60 Raman spectra taken from the maskelynite grains in our Zagami sample, no results of annealing were detected. Also, Zagami is reported to contain mesostasis that consists of intergrowths of silica and K-rich glass (shocked K, Na-feldspar) wherein the silica may be either cristobalite or "amorphous" [Duke, 1968]. We did not observe spectra of any glasses that were noticeably more siliceous than the maskelynite.

3.3. Olivine

Fayalitic olivine ($Fe_{90.96}$) has been reported at trace levels as part of an "intergrowth" assemblage in the late-stage DN lithology of Zagami, first noted by Mössbauer spectroscopic study [Vistisen *et al.*, 1992]. In our study, Raman spectra were taken from more than 300 points on the Zagami specimen, and we did not observe the characteristic peaks of olivine in any of them. As olivine is a strong Raman scatterer, we conclude that it is either absent from the areas we investigated or present at less than about a 0.33% abundance level.

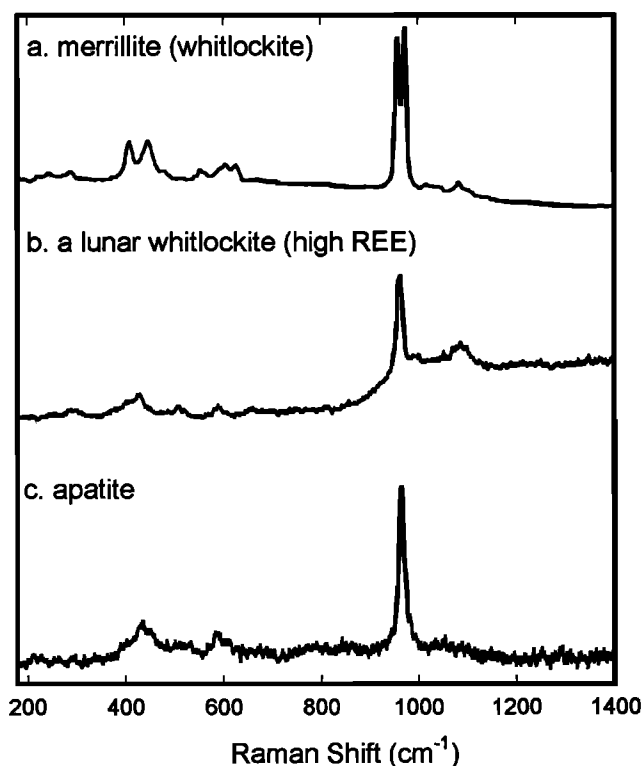


Figure 5. Typical Raman spectra of phosphates found in Zagami: (a) Zagami merrillite (whitlockite), (b) lunar whitlockite, and (c) Zagami apatite.

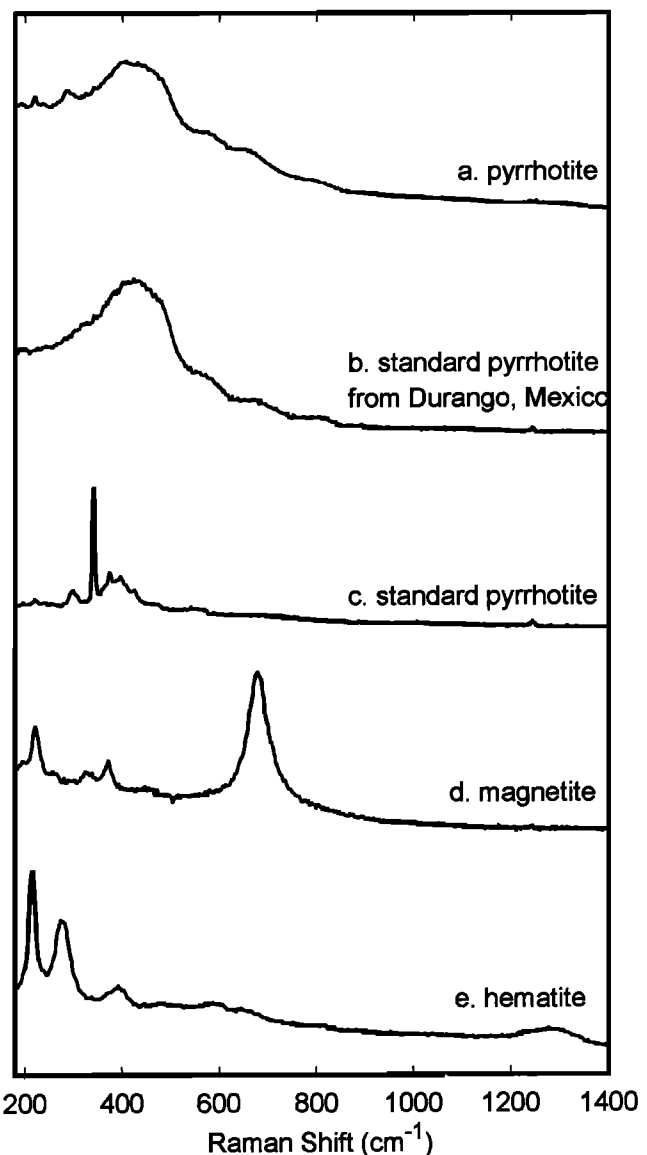


Figure 6. Typical Raman spectra of Fe-bearing mineral phases found in Zagami: (a) pyrrhotite, (b) a standard pyrrhotite, Durango, Mexico, (c) a standard pyrrhotite, (d) magnetite, and (e) hematite.

3.4. Phosphates

In the Zagami sample studied here, merrillite occurs as light-colored, narrow grains molded along the edges of maskelynite grains. The identification of phosphates by their Raman spectra is straightforward. Raman spectra were obtained for two accessory phosphates, merrillite (whitlockite), and apatite [see Prewitt and Rothbard, 1975; Jolliff *et al.*, 1996]; Figure 5 shows typical examples of their spectra. The spectrum of Zagami merrillite shows a doublet at 975 and 962 cm^{-1} as the main peaks (Figure 5a), typical of merrillite with low concentrations of rare earth elements (REE). In contrast, merrillite studied in lunar samples (Figure 5b, 15273,2 lunar rock chip) has only a single main peak near 962 cm^{-1} and peaks at higher wavenumbers from rare earth fluorescence [Jolliff *et al.*, 1996]. The fluorescence peaks of the REE are not Raman signals but have wavelengths independent of the exciting wavelengths. Their position on the scale of Raman

shifts, however, depends on the laser wavelength. Only two grains of apatite were encountered (Figure 5c), and both were present within merrillite grains. Merrillite grains in the Zagami meteorite commonly contain elongate glass inclusions that have eutectic compositions, and several have been observed that also contain euhedral titanomagnetite and pyrrhotite grains [Stolper and McSween, 1979].

3.5. Pyrrhotite

Figure 6a shows Raman spectra obtained from the Fe-bearing mineral in the Zagami sample. Pyrrhotite is the only Fe-sulfide phase found among them. Pyrrhotite is a complicated Fe-S mineral with three different structures (hexagonal, monoclinic, and pseudo-rhombohedral), and 12 superstructures, depending on its Fe/S ratio and on conditions of its formation such as the temperature and cooling history [Scott, 1974]. In order to identify pyrrhotite from its spectrum found in the Zagami sample, we measured several grains each of two standard pyrrhotite samples that gave two very different spectral patterns. The spectrum of Figure 6b, taken from a pyrrhotite sample from Durango, Mexico, is similar to that from Zagami. This contrasts sharply with the spectrum in Figure 6c, which shows sharp peaks between 300 – 450 cm^{-1} , with the strongest at 341 cm^{-1} . The latter spectral pattern and the position of its main peak are consistent with expectations from the Raman spectra of other S-bearing minerals with highly regular cation-S bonding such as pyrite, marcasite, sphalerite, and chalcopyrite, all of which have sharp and narrow Raman peaks, mostly at Raman shifts below 400 cm^{-1} . The 341 cm^{-1} peak of pyrrhotite is consistent with vibration of Fe-S bonds, based on its similarity to the strongest peaks from marcasite, sphalerite, and pyrite. Such a spectrum requires good ordering among the atoms in the mineral.

Both spectra of Figure 6a and 6b have only a strong and broad Raman band centered near 430 cm^{-1} . The tentative interpretation for the spectral pattern of the Zagami and Durango pyrrhotites is that they have the superstructure 1c of the hexagonal structure, in which occupation of the octahedral sites by Fe atoms is disordered [Scott, 1974]. The consequent irregularity of Fe-S bonding yields a broad distribution of vibrational frequencies, and the broad band near 430 cm^{-1} is the envelope of their overlapping peaks. Hexagonal pyrrhotite is the only high-temperature structural form of pyrrhotite.

3.6. Magnetite

Magnetite was identified through its Raman spectrum (Figure 6d), which shows a major broad peak at $\sim 670 \text{ cm}^{-1}$ plus a few weaker peaks at lower wavenumbers. Titanomagnetite is the form observed petrographically [Stolper and McSween, 1979; Brearley, 1991]; we have not yet determined whether Raman spectroscopy can readily distinguish among different forms of magnetite.

3.7. Hematite

Raman spectra of hematite (Figure 5e) were obtained from many bright grains adjacent to some of the pyrrhotite grains (indistinguishable in binocular microscopic observation). Hematite was also encountered in the point-counting measurements on both the rough-sawn surface and the lightly polished surface. Hematite has not been reported in the Zagami meteorite, although its mineralogy has been characterized carefully [e.g.,

Stolper and McSween, 1979; Brearley, 1991; McCoy et al., 1992, 1995], so we are puzzled by its appearance. Heating of pyrrhotite in air would yield hematite, and the laser beam of the Raman spectrometer certainly adds heat, especially to an opaque mineral, but this does not seem to be responsible for the appearance of the hematite spectra, as good pyrrhotite (and magnetite) spectra were observed. The low power density and red (632.8 nm) laser excitation wavelength would not be expected to oxidize pyrrhotite or magnetite readily. Allowing the laser beam to dwell on pyrrhotite grains did not induce an observable change with time in the spectrum for that mineral. Possibly, the hematite is a metamorphic oxidation product resulting from conditions that the Zagami meteorite experienced, or it may have been produced during cutting and preparation of the sample. The frequent appearance of the spectra of hematite in the Zagami meteorite and some other materials we have tested remains a topic for further study.

4. Mineral Proportions

For those measurements in which points along a linear traverse or on a grid were sampled, the mineral identifications from the Raman spectra are roughly the equivalent of a petrographic point-count [Haskin et al., 1997]. Of the Raman measurements made on the unpolished and the lightly polished sawn surfaces of the Zagami sample, 302 were collected in this manner. The total scanning distances for each line or grid traverse were long enough (0.5 – 1.0 cm) to exceed the scale of heterogeneity of the sample, so the mineral mode obtained from the measurements should be representative, within the statistics of that number of points observed. Spectral quality for mineral identification was essentially the same on the rough-sawn surface as on the lightly polished surface of this Zagami sample.

Table 1 shows the results of the Raman point-counting measurements. They are separated into two categories: with laser beam focusing adjustment at each measurement point and without. The scanning measurements along three traverses (90 points in total) were taken using a carefully focused laser beam and high magnification and high numerical aperture sampling objectives (80 \times , 0.85 NA; 50 \times , 0.85 NA). For these measurements, the sampled spots were smaller in diameter and the sampling depths were on average shallower than for the unfocused points, which were taken with a 20 \times , 0.4 NA objective. The rest of the rectangular grid-style measurements (212 points in total), taken in two separate areas, were obtained with the less condensed laser beam by using a 20 \times , long-working distance sampling objective. This latter objective is the type that would be used by a simple planetary instrument having a fixed sampling distance. As seen in Table 1, the two methods gave basically the same results. The proportions of pyroxene (74% and 76%) obtained by the both methods are identical within statistics. The same is true for maskelynite (21% and 20%). The modes are slightly different for the minor or accessory mineral phases (phosphates, oxides, and sulfides), which is statistically reasonable.

The mineral mode obtained from our traverse analyses is consonant with those from other petrographic studies that were done on different Zagami samples, as seen in Table 2. The Raman spectra do not include a category "mesostasis" because the spectrometer receives signal only from minerals that might be in mesostasis (discussed above). The phosphate minerals are a good example of this; the proportion of phosphate is similar to the pro-

Table 1. Results of Raman Point-Counting Measurements

	Pyroxene	Maskelynite	Merrillite	Apatite	Magnetite	Hematite	Pyrrhotite	Organic*	Total points
Fine beam with focusing adjustment									
40 points traverse 1/S/Sunp**/100 μ m step	29	7	0.5			2	1.5		40
24 points traverse 2/H1/Sunp/500 μ m step	17.5	5						1.5	24
26 points traverse 3/H1/Sunp/100 μ m step	16	6						4	26
Subtotal (frequency of encounter)	62.5	18	0.5			2	1.5	5.5	90
Percentage (excludes organic)	74.0	21.3	0.6			2.4	1.8		100.1
Coarser beam without focusing adjustment									
22x5 points grid 1/H2/Sp/ 200 μ m step	88.5	18	2.5		1				110
17x6 points grid 2/H2/Sunp/100 μ m step	73	24	2		2	1			102
Subtotal (frequency of encounter)	161.5	42	4.5		3	1			212
Percentage	76.2	19.8	2.1		1.4	0.5			100.0
Total (frequency of encounter)	224	60	5		3	3	1.5	5.5	302
Mineral proportions (exclude organic)	0.755	0.202	0.017		0.010	0.010	0.005		

* The organic phase in the Zagami sample was an impurity from handling; it was removed by light polishing of the specimen.

** S= S3000, 80x objective, H1= HoloLab, 50x objective, H2= HoloLab, 20x objective, Sunp= unpolished surface, Sp= polished surface

portion of mesostasis reported in the petrographic measurements. Nor is there a category for "shock melt." We presumed in our tabulation that all glassy spectra were maskelynite. We conclude that the Raman point counts give basically the same results as petrographic point counts, as observed for other materials [Haskin *et al.*, 1997].

5. Stand-Alone Characterization of a Martian Rock by Raman Spectroscopy

The Raman spectroscopic measurements were made in the laboratory using a spectrometer with an optical performance similar to one that would be suitable for on-surface planetary application [Wang *et al.*, 1998]. They were made using a similar measurement procedure, point-counting on a grid or along a line, as anticipated for mineral analysis on planetary surfaces [Haskin *et al.*, 1997]. If we had obtained these data from a rock on the surface of Mars, using Raman spectroscopy only, and we knew nothing else about this rock, what could we reasonably conclude just from analysis of the Raman spectra about the minerals and the rock type?

From the abundant pyroxene and the absence of lower-temperature minerals, we would know the rock was igneous, and from the absence of quartz and K-feldspar, we would conclude that it was not a felsic igneous rock. From the range and distribution of pyroxene compositions, we would know that the rock did not crystallize slowly in a plutonic setting. An equilibrated plutonic rock would have either a single pyroxene composition or

a bimodal distribution if it crystallized both low- and high-Ca pyroxene or if it had exsolved to produce lamellae, and such a pattern was not observed.

From the abundance of the glass, we would know the rock had either quenched or been shocked. The combination of abundant feldspathic glass along with pyroxene would suggest either a pyroxene-phyric lava or a pyroxene-plagioclase rock such as a gabbro or basalt with shocked plagioclase (maskelynite). The broad range of pyroxene composition is consistent with chemical zoning preserved during rapid crystallization and supports a basaltic texture; however, the frequency of adjacent pyroxene-only spectra along a linear traverse suggests relatively coarse pyroxene, i.e., phenocrysts. The relatively low Mg' of the most magnesian pyroxene makes basalt a better choice than a more feldspathic rock and the mode supports this, as described below. The presence of scattered phosphate minerals is consistent with the presence of areas of crystallized mesostasis. From the approximate position of the broad peak in the Raman spectra of glass, we would distinguish it as feldspathic, not an Fe-rich silicate melt as would be expected of glassy basaltic mesostasis. Thus we would conclude that the rock was sufficiently shocked to destroy its plagioclase.

From the modal analysis, we would know that the rock is rich in pyroxene and therefore mafic. It is considerably richer in pyroxene than typical mafic melts, whose chemical compositions lie on or near a plagioclase-pyroxene cotectic. This would mean that the melt was a high-temperature one, well into a pyroxene field of the phase diagram, or a cooler melt that had accumulated pyroxene. That nearly all of the pyroxene is monoclinic restricts the nature of the rock and its parent melt. Based on the Earth and Moon as analogs, the high abundance of pigeonite implies a high Ca/Al ratio typical of basalts, rather than the lower Ca/Al ratio characteristic of plagioclase-orthopyroxene plutonic rocks such as norites. Pyroxene is the only mafic mineral observed and therefore apparently the only mafic mineral that formed during crystallization of the parent melt. If we were to conclude that it is a basalt, the absence of olivine would constrain this rock to the field of tholeiites. The parent melt had a moderate, but not high Mg', because the Mg' of some of the pigeonite reaches ~0.7.

Suppose crystallization of the melt parental to the rock had progressed slowly, at least for a while, so that the Mg' of the pyroxene remained in equilibrium with that of the residual melt. As long as crystallization progressed in that manner, pyroxene of

Table 2. Comparison of Mineral Mode Obtained by Raman Traverses With Modes From Previous Studies

	This Study, vol%	Stolper and McSween [1979], vol%		McCoy <i>et al.</i> [1992], vol%			
				Fine Grained		Coarse Grained	
Pyroxene	75.5	76.3	69.7	77.7	74.3	76.0	80.4
Maskelynite	20.2	18.8	24.7	17.6	18.8	18.6	10.3
Mesostasis		1.7	2.6	1.8	3.0	2.1	3.7
Oxides	2.0	2.7	2.8	1.5	1.8	2.0	2.6
Sulfides	0.5	0.5	0.2	0.6	0.4	0.4	0.6
Phosphates	1.7			0.5	0.6	0.5	1.3
Shock melt				0.1	0.9	0.3	0.9

a single composition would be produced. The histogram of pyroxene (Figure 3b) is not that of a narrow, equilibrium composition. If crystal dimensions and diffusion rates prohibited complete equilibrium, yet cooling was still slow, the crystal would become zoned. As this occurred, the Mg' of the newly forming pyroxene would change only slowly at first because a relatively large volume of the melt would have to crystallize before the Mg' of the melt changed appreciably. The rate of change of Mg' would thus become more rapid as the relative proportion of melt in the system decreased. The zoning would approach that of surface equilibrium. The resulting histogram of pyroxene compositions would show a relatively high proportion of core pyroxene and a monotonically decreasing volume of pyroxene with decreasing Mg' for as long as the crystallization progressed smoothly and the Mg' was controlled primarily by pyroxene crystallization. This also is not observed (Figure 3b). Instead, most of the pyroxene has a relatively low Mg'. This suggests rapid crystallization of the pyroxene, without an approach to equilibrium between melt and crystals. Such rapid crystallization could accompany eruption of the parent magma onto the surface of Mars. The fairly steep but still somewhat gradual rise from a low value of Mg' to the most common value (Mg' ~0.45) suggests crystallization onto magnesian cores, with crystallization departing slowly from equilibrium crystallization to surface equilibrium (Rayleigh) crystallization, then accelerating to precipitate additional pyroxene at an increasing rate and without surface equilibrium, and finally rapid crystallization of the remaining pyroxene component in the melt, much too rapidly to approach equilibrium between the growing pyroxene and the residual melt. This zoning pattern is consistent with the histogram of Figure 3b.

From the details of the merrillite spectrum, we would conclude that the rock was not rich in REE, as no effect on the spectral peaks and no addition of rare-earth fluorescence was observed. Furthermore, the Raman peaks are sharp, not broad as in the case of lunar whitlockite where high concentrations of U and Th cause partial metamictization and peak broadening. From the appearance of magnetite, hematite, and pyrrhotite, the fugacities of oxygen and sulfur can be constrained. If the hematite were found on Mars, and we were able to establish that it was part of the igneous rock and not contamination by red dust, we would conclude that the sample had experienced an oxygen fugacity consistent with the hematite-magnetite buffer. (We suspect the hematite in our sample is a product of sample preparation, so such a conclusion is thus not justified based on our laboratory Raman data.) The absence of hydrated minerals constrains the conditions under which the rock formed and the environments in which it subsequently resided; for example, no hydrated amphibole was observed, indicating it was absent or scarce.

Thus we would conclude that the rock was likely a pyroxenophytic basalt, in a general sense, a common rock type on Earth and probably on Mars. Overall, this study demonstrates that considerable basic, first order information about a rock and its origin and environments can be obtained just from a Raman spectroscopic study of its minerals. Obtaining such information in situ on a planetary surface requires a capable Raman spectrometer, a good means for its deployment, and that the surface of the rock be accessible. Dust was present on the rocks observed by the Pathfinder and Viking missions [Golombek et al., 1997; Binder et al., 1977; Mutch et al., 1977]. This dust did not cover most rocks uniformly, and the sensor of the spectrometer could possibly be guided to a relatively dust-poor location. Spectra at some

locations along a point-count traverse might be those of the dust, but many or most would not, and once the Raman spectra of the dust had been determined, the affected points could be ignored. More serious would be coatings corresponding to relatively thick desert varnish [Israel et al., 1997]. Such coatings are likely to be thin or absent in at least some areas (note the fluting on some of the rocks in the images from the Pathfinder mission; M. P. Golombek, personal communication, 1998), and the coatings can also be characterized and their effects can be taken into account. Besides, information on the nature of the coatings is valuable as information on past history and environments.

Given samples of the quality of the Zagami meteorite to analyze, Raman spectroscopy as a stand-alone technique provides considerable information for future planetary missions. The knowledge gained from that method can be enriched, however, by using it synergistically with other methods such as Mössbauer spectroscopy, thermal emission spectroscopy, and alpha-proton-x-ray spectroscopy.

Acknowledgments. We are grateful to T. Wdowiak of the University of Alabama at Birmingham for lending us the sample of the Zagami meteorite, and for partial support of this work by NASA under grants NAG 5-4642 and NAG 5-7140.

References

- Binder, A. B., R. E. Arvidson, E. A. Guinness, K. L. Jones, E. C. Morris, T. A. Mutch, D. C. Pieri, and C. Sagan, The geology of the Viking lander 1 site, *J. Geophys. Res.*, **82**, 4439–4451, 1977.
- Brearley, A. J., Subsolidus microstructures and cooling history of pyroxenes in the Zagami shergottite (abstract), *Lunar Planet. Sci.*, **22**, 135–136, 1991.
- Dele-Dubois, M. L., P. Dhameincourt, and H. J. Schubnel, Etude par spectroscopie Raman d'inclusions dans les diamants, saphirs et émeraudes/2, *Rev. Gemm.*, no. 64, 13–16, 1980.
- Duke, M. B., The Shergotty Meteorite: Magmatic and shock metamorphic features, in *Shock Metamorphism of Natural Materials*, edited by B. M. French and N. M. Short, pp 612–621, Mono Book Corp., Baltimore, 1968.
- Ghose, S., N. Choudhury, S. L. Chaplot, C. P. Chowdhury, and S. K. Sharma, Lattice dynamics of Raman spectroscopy of protoenstatite Mg₂Si₂O₆, *Phys. Chem. Miner.*, **20**, 469–477, 1994.
- Golombek, M. P. et al., Overview of the Mars pathfinder mission and assessment of landing site predictions, *Science*, **278**, 1743–1748, 1997.
- Haskin L. A., A. Wang, K. M. Rockow, B. L. Jolliff, R. L. Korotev, and K. M. Viskupic, Raman spectroscopy for mineral identification and quantification for in situ planetary surface analysis: A point count method, *J. Geophys. Res.*, **102**, 19293–19306, 1997.
- Heymann, D., Raman study of experimentally shocked plagioclase (abstract), *Lunar Planet. Sci.*, **23**, 421–422, 1987.
- Heymann, D., Luminescence of experimentally shocked plagioclase feldspar (abstract), *Lunar Planet. Sci.*, **19**, 489–490, 1988.
- Israel, E. J., R. E. Arvidson, A. Wang, J. D. Pasteris, and B. L. Jolliff, Laser Raman spectroscopy of vanished basalt and implications for in-situ measurements of Martian rocks, *J. Geophys. Res.*, **102**, 28705–28716, 1997.
- Jolliff, B. L., J. J. Freeman, and B. Wopenka, Structural comparison of lunar, terrestrial, and synthetic whitlockite using laser Raman microprobe spectroscopy (abstract), *Lunar Planet. Sci.*, **27**, 613–614, 1996.
- Marti, K., J. S. Kim, A. N. Thakur, T. J. McCoy, and K. Keil, Signatures of the Martian atmosphere in glass of the Zagami meteorite, *Science*, **267**, 1981–1984, 1995.
- McCoy, T. J., G. J. Taylor, and K. Keil, Zagami: Product of a two-stage magmatic history. *Geochim. et Cosmochim. Acta*, **56**, 3571–3582, 1992.
- McCoy, T. J., M. Wadhwa, and K. Keil, Another new lithology and a complex near-surface magmatic history (abstract), *Lunar Planet. Sci.*, **26**, 925–926, 1995.
- McMillan, P., Structural studies of silicate glasses and melts -- applications and limitation of Raman spectroscopy, *Am. Mineral.*, **69**, 622–644, 1984.

- Meyer, C., Mars Meteorite Compendium – 1996, JSC Rep. 27672, pp. 43–50, Johnson Space Cent., Houston, Tex., 1996.
- Mikouchi, T., M. Miyamoto, and G. McKay, Shocked plagioclase in martian and lunar meteorites: Textures, chemical compositions, Raman spectra, and implications for their post-shock thermal histories, papers presented to the Twenty-Third Symposium on Antarctic Meteorites, National Institute of Polar Research, Tokyo, 1998.
- Mutch, T. A., R. E. Arvidson, A. B. Binder, E. A. Guinness, and E. C. Morris, The geology of the Viking lander 2 site, *J. Geophys. Res.*, **82**, 4452–4467, 1977.
- Prewitt, C. T., and D. R. Rothbard, Crystal structures of meteoritic and lunar whitlockites (abstract), *Lunar Planet. Sci.*, **6**, 646–648, 1975.
- Scott, S. D., Sulfide phase equilibria, in *Sulfide Mineralogy*, Short Course Notes, vol. I, edited by P. H. Ribbe, Mineral. Soc. Am., Washington, D. C., 1974.
- Sekita, M., H. Ohashi, and S. Terada, Raman spectroscopic study of clinopyroxenes in the system CaScAlSiO_6 - $\text{CaAl}_2\text{SiO}_6$, *Phys. Chem. Miner.*, **15**, 319–322, 1988.
- Sharm, S. K., B. Simons, and H. S. Yoder Jr., Raman study of anorthite, calcium Tschermak's pyroxene, and gehlenite in crystalline and glassy states, *Am. Mineral.*, **68**, 1113–1125, 1983.
- Stöffler, D., Deformation and transformation of rock-forming minerals by natural and experimental shock processes, II, Physical properties of shocked minerals, *Fortschr. Mineral.*, **51**, 256–289, 1974.
- Stolper, E. M., and H. Y. McSween Jr., Petrology and origin of the Shergottite meteorites, *Geochim. Cosmochim. Acta*, **43**, 1475–1498, 1979.
- Treiman, A. H., Amphibole and hercynite spinel in Shergotty and Zagami: Magmatic water, depth of crystallization, and metasomatism, *Meteoritics*, **20**, 229–243, 1985.
- Treiman, A., and P. Treado, Martian maskelynite? Raman spectra of plagioclase-composition glasses from ALH84001, EETA79001, and ALHA77005, *Lunar Planet. Sci.*, **29**, #1196, 1998.
- Tschermak, G., Die meteoriten von Shergotty und Gopalpur, *Situngsber. Akad. Wiss. Wien Math., Naturwiss. Kl. Abt. I*, **65**, 122–146, 1872.
- Vistisen, L., D. Petersen, and M. B. Madsen, Mössbauer spectroscopy showing large-scale inhomogeneity in the presumed Martian meteorite Zagami, *Phys. Scr.*, **46**, 94–96, 1992.
- Wang, A., B. L. Jolliff, and L. A. Haskin, Raman spectroscopy as a method for mineral identification on lunar robotic exploration missions, *J. Geophys. Res.*, **100**, 21189–21199, 1995.
- Wang, A., B. L. Jolliff, K. M. Viskupic, and L. A. Haskin, Raman spectroscopic characterization of different types of pyroxene (abstract), *Lunar Planet. Sci.*, **28**, 1491–1492, 1997.
- Wang, A., L. A. Haskin, and E. Cortez, A Raman spectroscopic sensor for in situ mineral characterization on planetary surface, *Appl. Spectrosc.*, **52**, 477–487, 1998.
- Watson, L. L., I. D. Hutcheon, S. Epstein, and E. M. Stolper, Water on Mars: Clues from deuterium/hydrogen and water contents of hydrous phases in SNC meteorites, *Science*, **265**, 86–90, 1994.

L. A. Haskin, B. L. Jolliff, and A. Wang, Department of Earth and Planetary Sciences, Campus Box 1169, Washington University, One Brookings Drive, St. Louis, MO 63130. (alianw@levee.wustl.edu)

(Received November 2, 1998; revised January 26, 1999; accepted January 27, 1999.)